RSC Advances

PAPER

View Article Online
View Journal | View Issue

Cite this: *RSC Adv.*, 2025, **15**, 22076

Received 10th September 2024
Accepted 13th June 2025

DOI: 10.1039/d4ra06524g

rsc.li/rsc-advances

Highly selective catalytic pathway utilizing metal oxide nanoparticles to produce formic acid through methanol oxidation

Mina Arshad, *[a] Iram Mahmood,[b] Ali Sarosh,[a] Asim Umer,[a] Muhammad Athar[a] and Mahboob Ahmed Aadil[a]

An emerging alternative energy source is formic acid, which has low toxicity and high hydrogen-carrying capacity. Metal-containing nanoparticles are very attractive for many applications, allowing large-scale and environmentally friendly production. This study proposes liquid-state synthesis for clean and facile formic acid production *via* methanol oxidation over metal oxide nanoparticles. MoO_3, Fe_2O_3, TiO_2 and V_2O_5 nanocatalysts were prepared through sol–gel, solvothermal, reflux condensation and ball milling techniques, respectively, and their efficacy in formic acid production *via* methanol oxidation was assessed. The synthesized nanoparticles were further characterized through scanning electron microscopy, energy dispersive X-ray spectroscopy and X-ray diffraction. The performance of laboratory-prepared nanoscale metal oxide catalysts for formic acid production was evaluated through batch reactions under ambient temperature and pressure conditions to enhance energy efficiency and maximize conversion. Formic acid was quantitatively analyzed using high-performance liquid chromatography (HPLC). Results revealed that the nanocatalysts considerably promoted the generation of formic acid, especially MoO_3, which provided a 91% product acid yield, which was the greatest among the other nanocatalysts under the employed reaction conditions.

1 Introduction

Formic acid is one of the most valuable and competent green organic acids that is not easily substituted in certain applications, mainly as a preservative in food products and antibacterial agent in livestock feed.[1] In leather manufacturing, formic acid is used for tanning, fixing dyes, and finishing textiles because of its acidic nature. In textile processing, formic acid is used as a neutralizing agent to adjust the pH during the treatment steps.[2] It is used to adjust the pH during flue gas desulfurization.[3] In the synthesis of epoxidized soybean oil, formic acid is used in combination with hydrogen peroxide as an oxidizing agent.[4]

Most interestingly, formic acid is undergoing rapid advancements to overcome the energy crisis caused by conventional fossil fuels and is projected to be used as direct formic acid fuel cells for future portable equipment and automobile applications.[5] Moreover, formic acid is industrially utilized as a detergent and cleanser for powerful descaling. Formic acid is an immensely versatile chemical with extensive application. Formic acid is widely used in agriculture for crop protection and as an industrial chemical. It is also used as a coagulant in many rubber manufacturing industries and latex coagulation.[6] Formic acid is also used in the pharmaceutical industry as an active ingredient in the production of different pharmaceutical products. Medically, it is used for the treatment of warts.[7]

Through the oxidation of wet biomass, formic acid yields of 20–75% can be achieved.[8] This process involves aqueous catalytic oxidation to convert biomass such as wood, waste paper, and sugar into formic acid with CO_2 as a byproduct. However, because of the low yield of formic acid, this process is not usually preferred, and biomass oxidation does not fulfill the industrial and domestic requirements of formic acid.

The catalytic hydrogenation of carbon dioxide is also used to synthesize formic acid. Homogeneous catalysts have been used in this process.[9] However, the main drawback of this process is that the reaction moves in the backward direction, and the reaction is at equilibrium with reactants, which reduces the efficiency of this process. Therefore, to improve this process, additional separation steps for formic acid are required, which increases the cost of this process. Moreover, a large amount of CO_2 is not easy to transport because of environmental issues.

Industrially, the production of formic acid is carried out through methyl formate. Initially, when methanol reacts with carbon monoxide (CO) in the presence of a base, methyl formate is obtained.[10] The reaction occurs at elevated pressure. The

---

[a] *Department of Chemical Engineering, Muhammad Nawaz Sharif University of Engineering and Technology, Multan, Pakistan. E-mail: minaarshad@mnsuet.edu.pk; me.mina34@yahoo.com*

[b] *University of Bolton, Islamabad, Pakistan*

obtained methyl formate is treated further in two ways to produce formic acid on an industrial scale. First, during the direct hydrolysis of methyl formate, the reaction occurs in the presence of excess water to produce formic acid. Consequently, methanol and formic acid are obtained. In another method to synthesize formic acid, the obtained methyl formate is first reacted with ammonia to give formamide. The formamide is then hydrolyzed in the presence of sulfuric acid to produce formic acid. However, during the reaction, ammonium sulfate is also produced as a by-product, which is hazardous and not easy to handle. Therefore, these two routes for formic acid production are not generally favourable because direct hydrolysis of methyl formate requires an excess amount of water, which is not cost-effective, and the hydrolysis of formamide produces hazardous by-products whose handling is a major issue. Recently, the formation of methyl formate has also been practised through the electron irradiation process of methanol and carbon monoxide,[11] which can be converted to formic acid. Efforts to increase CO_2 to HCOOH electrochemical reduction have been given high focus in research over the past several decades. Formic acid produced from CO_2 *via* electrochemical reduction using electrocatalysts has great potential.[12] A very effective technique employing bimetallic alloy catalysts for CO_2 electro-reduction to formic acid is also proposed.[13]

Recently, a new and environmentally acceptable gas phase method for formic acid production was introduced. In their work, commercially annulated iron and molybdenum catalysts were used for the oxidation of methanol to formaldehyde. For further conversion of formaldehyde to formic acid, vanadium and titanium catalysts were used in the shape of the pellets. Because this reaction is highly exothermic, a tubular reactor was used for this purpose. The resulting gas product from the reactor was condensed, and formic acid, water, and residual formaldehyde were obtained as the final product. The condensate showed a formic acid content of up to 55–62 wt%.[14] The yield of the formic acid produced is low. This process is not very economical and efficient because of the use of larger-sized catalysts in the mm range. An additional cost is required for evaporation and then cooling the system.

In general, the process of producing formic acid from CO_2 has detrimental effects on the environment, primarily in the form of greenhouse gas emissions. An effective approach for reducing greenhouse gas (GHG) emissions and the depletion of fossil fuel resources is carbon capture and utilization (CCU) technology. A potential CCU method is the CO_2-based synthesis of formic acid (FA) using H_2. Additionally, the impact on global warming can be lowered by 95.01% by synthesizing FA through CO_2 hydrogenation.[15] Recently, a novel approach utilizing a magnesia catalyst through direct hydration to produce formic acid has been introduced.[16]

In recent research findings, formic acid synthesis using electrocatalysis,[17] heterogeneous catalysis and its feasibility for energy applications are presented.[18] Many approaches, including physical, chemical, and biological methods, have been employed in nanoparticle production. For the past ten years, the "clean" production of metal and metal oxide nanoparticles has been a very interesting research area. To synthesize uniformly sized nanoparticles with long-term stability, physical and chemical methods are generally believed to be the best.[19]

Transition metal oxide nanoparticles are considered efficient for methanol oxidation catalysis owing to their higher selectivity towards desired products and multiple chemical intermediates.[20] The present work is an economical and safe route for formic acid production through the photocatalytic oxidation of methanol in the liquid phase using metal oxide nanoparticles. Photocatalytic activity is enhanced owing to the greater surface-to-volume ratio of nanoparticles compared with their respective counterparts in larger dimensions.[21] The photocatalytic oxidation reaction is stimulated by UV radiation, thereby providing energy and facilitating the synthesis of formic acid. In this regard, metal oxide nanoparticles serve as efficient photocatalysts by enhancing the activity of UV radiation in oxidation reactions. Nanoparticles, such as titania, enhance charge transfer mechanisms and boost reaction rates when exposed to UV light, which makes it easier to convert methanol to formic acid. In this work, four metal oxide catalysts, namely molybdenum oxide, iron oxide, titanium oxide, and vanadium oxide, are used in the nanometric range. Nanocatalysts can enhance the reaction rate while having at least one nanoscale dimension. Moreover, nano-structured catalysts are expected to have more chemical, optical, and electronic properties. For nanocatalysts, the increasing surface-to-volume ratio with decreasing particle size strongly increases the particular catalytic activity, which also helps in the case of methanol oxidation to formic acid. This process is energy efficient and more reactive and modifies the previously used methods of manufacturing in a safe and green way, with a good yield of formic acid. This work is limited in considering the common part of Fe_2O_3 using the solvothermal method, while MoO_3, V_2O_5, and TiO_2 were synthesized using the sol–gel method for comparison. This study observed that the production of formic acid *via* methanol oxidation is heavily influenced by the choice of catalyst, as different catalysts exhibit different performances owing to their varied sizes and crystalline structures on a specific reaction path. Therefore, these factors should be considered in future studies.

2 Experimental

2.1 Nanocatalyst preparation

2.1.1 Synthesis of molybdenum oxide nanoparticles. The sol–gel method was adopted to synthesize molybdenum oxide (MoO_3) nanoparticles. The schematic diagram is depicted in Fig. 1a. First, 1.16 g ammonium molybdate powder was dissolved in 10 ml of de-ionized water. Then, 0.38 g citric acid prills were mixed into this solution using a magnetic stirrer. To obtain a pH of 7, 3 to 4 drops of ammonium hydroxide were added dropwise to the mixture. The solution was then heated in an oven at 250 °C for 1 h. A gel was obtained at that point. Then, it was placed in a muffle furnace at 500 °C for more than one hour. The powder was then dried in a vacuum oven overnight at 45 °C to remove the moisture present.

2.1.2 Synthesis of iron oxide nanoparticles. A solvothermal route was taken to synthesize the iron oxide (Fe_2O_3) nanoparticles. Almost 1.4 g ammonium persulfate $(NH_4)_2S_2O_8$ was

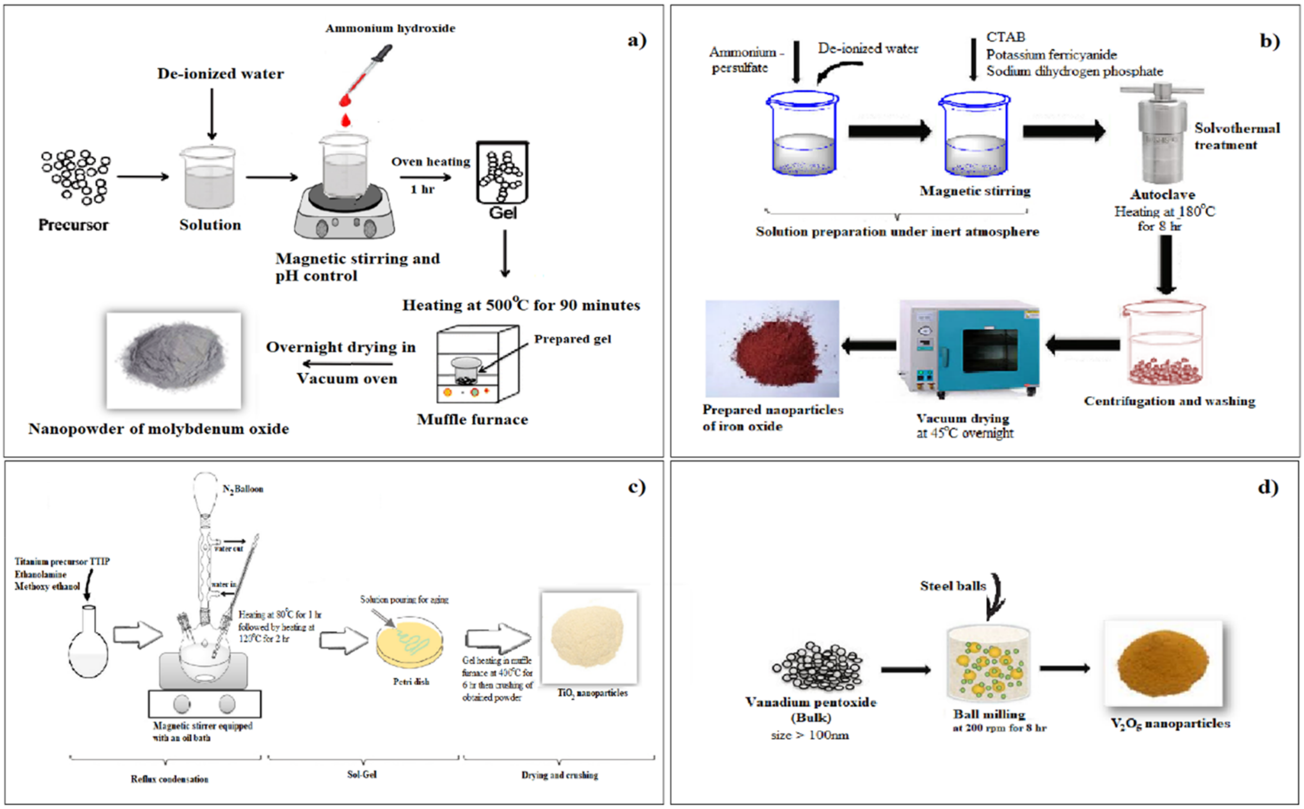

Fig. 1 Schematics of the synthesis of metal oxide nanoparticles: (a) molybdenum trioxide (MoO_3) nanoparticles. (b) Ferric oxide (Fe_2O_3) nanoparticles. (c) Titanium dioxide (TiO_2) nanoparticles. (d) Vanadium pentoxide (V_2O_5) nanoparticles.

dissolved in 100 ml de-ionized water. Then, 0.02 g CTAB and 0.42 g potassium ferricyanide $K_3[Fe(CN)_6]$ were mixed in the solution using a magnetic stirrer. A very small quantity of 0.002 g sodium dihydrogen phosphate was also added to the mixture. All this experiment was performed in an inert atmosphere. Initially, a yellowish-coloured solution was obtained. The solution was heated in an oven at 180 °C for 8 h using an autoclave. Centrifugation was carried out on the obtained solution after heating. After decanting the solvent, the sample was washed twice with methanol and ethanol. The obtained sample was then heated in a vacuum oven overnight at 45 °C. Reddish powder was obtained as a product. A schematic diagram of the process is depicted in Fig. 1b.

2.1.3 Synthesis of titanium oxide nanoparticles. The sol–gel procedure was followed to prepare the titania nanoparticles. 25 ml of the precursor titanium tetra isopropoxide (TTIP), 12.5 ml ethanolamine, and 100 ml methoxy-ethanol were added and stirred for 1 h at ambient temperature under an inert atmosphere. The temperature was increased to 80 °C, and stirring was continued for 1 h. The temperature was increased to 120 °C, and stirring was continued for 2 h. Subsequently, a wine-coloured solution was obtained. The solution was poured into Petri dishes for ageing in the presence of atmospheric oxygen until the time of gel formation, as shown in Fig. 1c. The obtained gel was kept in a muffle furnace for heating at 400 °C. The obtained powder was crushed in a mortar and piston to obtain fine particles.

2.1.4 Synthesis of vanadium oxide nanoparticles. The size of the bulk vanadium pentoxide powder was reduced by ball milling. 15 g of powder vanadium oxide was placed in the sampler for ball milling at 200 rpm for 7 h. Balls were used in the sampler for size reduction through compression, impact, and attrition. Nanoparticles were obtained after ball milling the sample, as shown in Fig. 1d.

2.2 Characterization

All the prepared catalysts were characterized using a scanning electron microscope (JEOL JSM-6460) to check their morphology and particle size. X-ray diffraction (JEOL JDX-II) was performed to identify the phase and crystal system of the nanoparticles by CuKα ($\lambda = 1.5406$ Å) at ambient temperature. All four prepared nanoparticles were monitored at the 2 theta range of 20°–80° in XRD analysis. For elemental composition analysis, an energy-dispersive X-ray spectrometer (JEOL JED-2300) was used for each prepared catalyst. Afterwards, high-performance liquid chromatography (PerkinElmer, Series 200) was performed to monitor the presence of peaks of formic acid.

2.3 Catalytic oxidation of methanol under UV-light

UV light has a shorter wavelength than visible light and can successfully be used for methanol oxidation reactions to produce formic acid. Overall, energy requirements decrease in

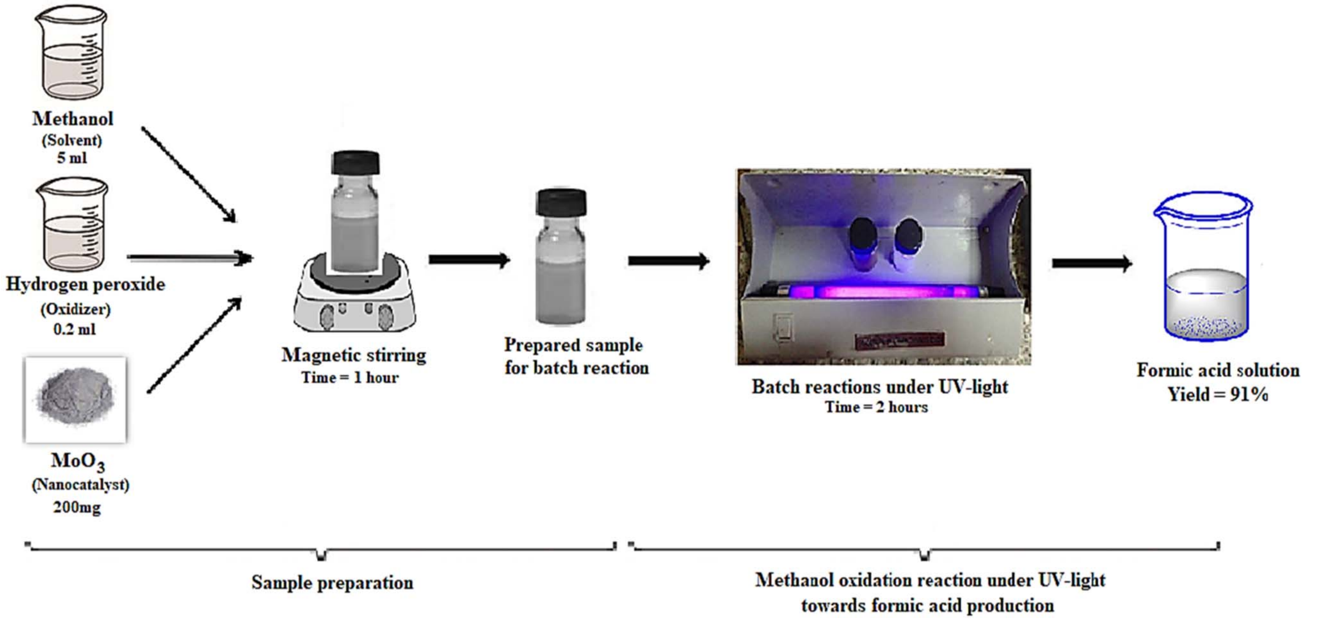

Fig. 2 Schematics of batch reactions for methanol oxidation using the molybdenum trioxide nanocatalyst under UV-light (same reaction mechanism was followed for other samples containing iron oxide, titanium dioxide and vanadium pentoxide nanocatalysts).

the presence of a catalyst, and under UV light, the reaction becomes more efficient and productive.

Batch reactions are performed to check the catalytic activity of nanocatalysts towards formic acid production, as shown in Fig. 2. The wavelength of the UV lamp used to conduct the batch reaction is 357 nm. Table 1 shows the values of various reaction parameters, such as the quantity of catalysts, solvent methanol, oxidizing agent H_2O_2, time for UV degradation, and time for stirring. For any catalytic reaction, the sizes, materials and crystalline structures of catalysts directly influence the overall reaction performance in terms of selectivity, catalytic activity and stability. The comparison of the four metal oxide nanoparticles is made for the main catalytic methanol oxidation reaction. In this regard, various reaction parameters, such as the amount of catalyst, reaction phase, time for reaction under UV-radiation and the amount of alcohol and oxidizing agent, as depicted in Table 1, are kept constant to serve as a control for better catalytic comparison under ambient temperature and pressure conditions. The basis for parametric amounts in Table 1 is by weight for solid catalysts and by volume for liquid alcohol and oxidizing agents.

It is an important perspective that catalyst composition significantly impacts the reaction kinetics of methanol oxidation to formic acid, affecting both the selectivity and activity of the process. A thorough comprehension of the reaction mechanism and surface customization is necessary for the development of a selective catalyst.[22] The catalytic oxidation of methanol under UV light using prepared nano-catalysts (molybdenum trioxide, titania, iron oxide and vanadium pentoxide) has been explored to optimize this reaction. The reason is that the choice of catalyst can alter the reaction pathway by enhancing the reaction rate and improving the formic acid yield.

The catalytic oxidation of methanol employing a molybdenum trioxide (MoO_3) catalyst has high activity in producing formic acid. Molybdenum metal possesses five oxidation states that are readily accessible and a rich coordination chemistry, along with its refractory nature, making molybdenum an excellent candidate for use as a heterogeneous catalyst. The mechanism for catalytic oxidation involves the formation of surface alkoxides over a molybdenum trioxide catalyst. Moreover, titania (TiO_2), a well-known photocatalyst, assists in the alcoholic oxidation pathway by first causing methanol to dehydrogenate into formaldehyde and then continuously oxidizing it to formic acid.[23] In comparison, titanium dioxide catalysts and iron oxide (Fe_2O_3) catalysts exhibit higher activity

Table 1 Values of reaction parameters for batch reactions under UV light

Catalyst	Catalyst quantity (mg)	Methanol (ml)	H_2O_2 (ml)	Time under UV lamp (h)	Time for stirring (h)
MoO_3	200	05	0.20	02	01
Fe_2O_3	200	05	0.20	02	01
TiO_2	200	05	0.20	02	01
V_2O_5	200	05	0.20	02	01

and a higher yield of formic acid. The formaldehyde formation involves the activation of methanol through acidic sites; the possibility of this activation primarily determines oxidation activity. The combination of metal oxides contributes to the acidic property's enhancement or modification. Selective oxidation is determined by an acid–base-type interaction between the catalyst surface and the organic material to be oxidized; the results of methanol and Fe_2O_3 catalysts have shown good acid–base properties. Similarly, the vanadium pentoxide (V_2O_5) nanoparticles have also significantly converted the methanol by multiple electron transfer and high solubility during the catalytic oxidation process, resulting in considerable conversion and a tendency to increase the product yield.

3 Results and discussion

3.1 Morphological and chemical analysis of prepared nanoparticles

3.1.1 Morphological structures and size range of prepared metal oxide catalysts. Morphological structures of the molybdenum oxide nano-catalyst were observed through SEM. SEM images showed that the molybdenum oxide nanoparticles were fairly spherical, as reported by Nitin and Anandgaonker.[24] The size range was from 44 nm to 92 nm. The average particle size of the nanoparticles was 68 nm, as shown in Fig. 3a. SEM images showed some aggregated particles of MoO_3 caused by the high-temperature treatment in the muffle furnace (exceeding 500 °C) during the synthesis and drying processes. Therefore, the optimized temperature of 500 °C showed fewer aggregated particles.

The SEM images showed that the iron oxide nanoparticles were spherical, as shown in Fig. 3b. The average particle size of iron oxide nanoparticles was 18 nm, varying from 10 nm to 26 nm.

SEM images of titanium dioxide nanoparticles showed spherical morphology. Agglomerated particles were also observed in addition to individual nanoparticles owing to the high-temperature treatment applied during the synthesis and drying process and the conversion from gel to powder. The particle size was detected from 16 nm to 23 nm. Thus, the average size observed through SEM images was 20 nm, as shown in Fig. 3c. Titania, as a photocatalyst, is affected by the presence of agglomerates and aggregates in terms of a decrease in the fraction of light absorbed. Photoactivity is affected by the cluster formation of photocatalysts. Moreover, at the particle-to-particle level, agglomeration or aggregation may result in the creation of new surface states that alter the quantum yield and photon absorption in ways unrelated to the main characteristics of the nanoparticles.

The vanadium oxide nanoparticles presented by the SEM image in Fig. 3d were well dispersed and spherical. These nanoparticles ranged from 13 nm to 23 nm. The average particle size of vanadium oxide nanoparticles was observed as 18 nm.

3.1.2 Elemental composition analysis of prepared metal oxide catalysts. The elemental composition of the prepared catalysts was determined using an energy-dispersive X-ray spectrometer (EDS). The EDS spectrum of molybdenum trioxide nanoparticles shows the presence of Mo and O in the prepared sample along with no impurities present. The peaks of molybdenum and oxygen along with the weight and mass percentages are presented in Fig. 4a. Similarly, the spectrum result of iron oxide nanoparticles shows the presence of Fe and O in synthesized nanoparticles, along with elemental composition in weight and atomic percentage, as presented in Fig. 4b.

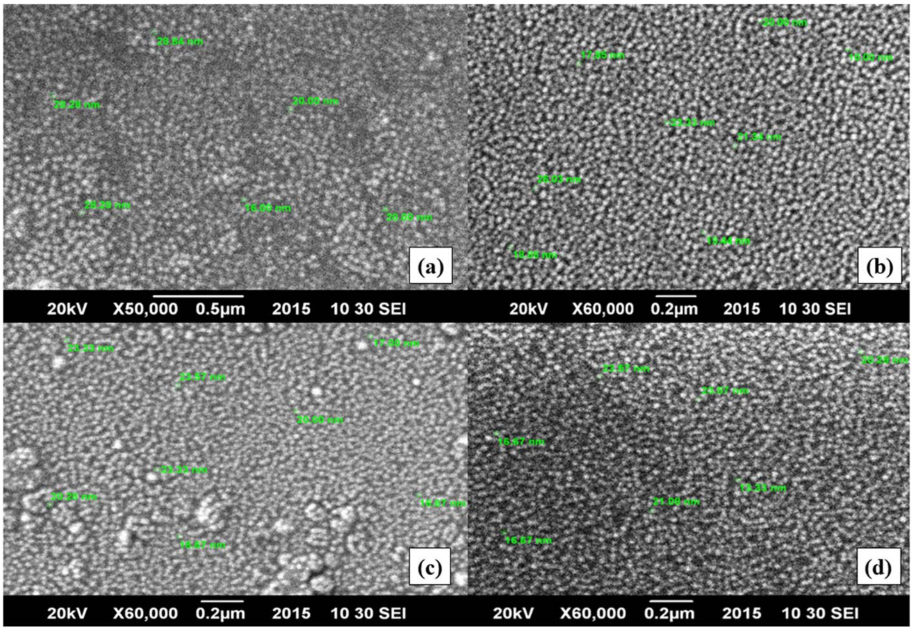

Fig. 3 SEM micrographs of the prepared nanoparticles: (a) molybdenum trioxide (MoO_3) nanoparticles. (b) Iron oxide (Fe_2O_3) nanoparticles. (c) Titanium oxide (TiO_2) nanoparticles. (d) Vanadium pentoxide (V_2O_5) nanoparticles.

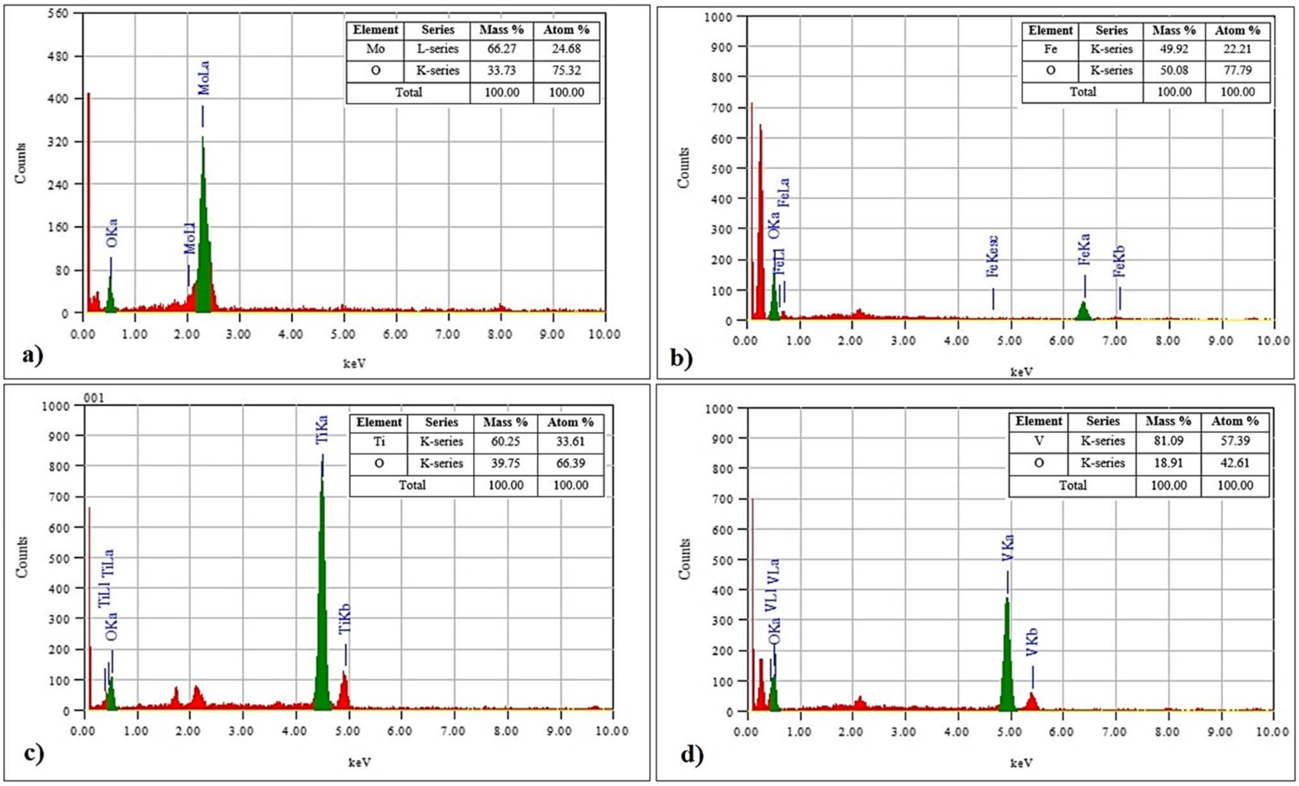

Fig. 4 EDS spectrums along with mass and atomic percentages of (a) molybdenum trioxide nanoparticles, (b) iron oxide nanoparticles, (c) titanium dioxide nanoparticles and (d) vanadium pentoxide nanoparticles.

In the same manner, Fig. 4c and d depict the EDS spectra of titanium oxide and vanadium pentoxide, respectively, along with their elemental composition in weight and atomic percentages.

3.2 Structural and phase analysis of prepared metal oxide catalysts

Using CuKα ($\lambda = 1.5406$ Å) at room temperature, the crystal structure and phase analysis of the catalyst samples generated in the lab were examined using an XRD pattern. All of the sample indexed XRD patterns are displayed in Fig. 5a–d in the 2-theta range of 20°–80°. Fig. 5a shows an orthorhombic crystal system and confirms the appearance of MoO_3, with characteristics (021), (110), (040), (111) and (020) (reference code 00-005-0508). The deformations in the crystal structure of the MoO_3 from a cubic crystalline nature to orthorhombic have been attributed to the concentration of the element. The XRD analysis of molybdenum oxide powder showed the orthorhombic structure of the prepared nanoparticles, which resembled the nanoparticles prepared by Dighore and Anandgaonker.[24] Moreover, the analysis confirms the crystal structure to be orthorhombic of MoO_3 as given by Mamatha and Murthy *et al.*[25]

The XRD pattern of Fe_2O_3 revealed a rhombohedral crystal with nanoparticles that were hematite with distinct peaks *hkl* positions (104), (110), (116), (012) and (024) represented under reference code 00-024-0072, as shown in Fig. 5b.

Similarly, the distinctive peaks of anatase TiO_2 are depicted in Fig. 5c at respective 2θ positions and are represented by the *hkl* planes (101), (004), and (200), confirming the anatase phase of titanium oxide nanoparticles (XRD JCPDS card no. 78-2486).[26]

The recorded XRD pattern in Fig. 5d depicted a well-crystalline sample and showed the presence of V_2O_5, with characteristic (001), (101), (110), (301), and (020) planes at corresponding 2θ positions confirmed by JCPDS card no. 41-1426, confirming the presence of V_2O_5, as also prepared by Saqib Rafique and Shahino Mah Abdullah *et al.*[27] The calculated density (g cm^{-3}), volume of cell (10^6 pm^3), and crystallite size through Scherrer's equation are presented in Table 2.

The XRD technique was used to measure the crystallite size by neglecting the amorphous part. As an outcome, XRD's three-dimensional structure showed larger crystallite size due to selected domains, specifically for Fe_2O_3, TiO_2 and V_2O_5 nanoparticles, as depicted in Table 2. Similarly, the crystalline size of a catalyst can exceed its particle size owing to the structural characteristics and synthesis methods employed during the preparation of Fe_2O_3, TiO_2 and V_2O_5. This phenomenon is particularly found in heterogeneous catalysis; consequently, the relationship between crystallite and particle size can significantly influence catalytic performance. For example, in some cases, catalysts are designed as single crystals, where the entire particle is a single crystal. Here, the crystalline size equals the particle size. In heterogeneous catalysts, both the selectivity and activity are strongly correlated with the geometric structure and

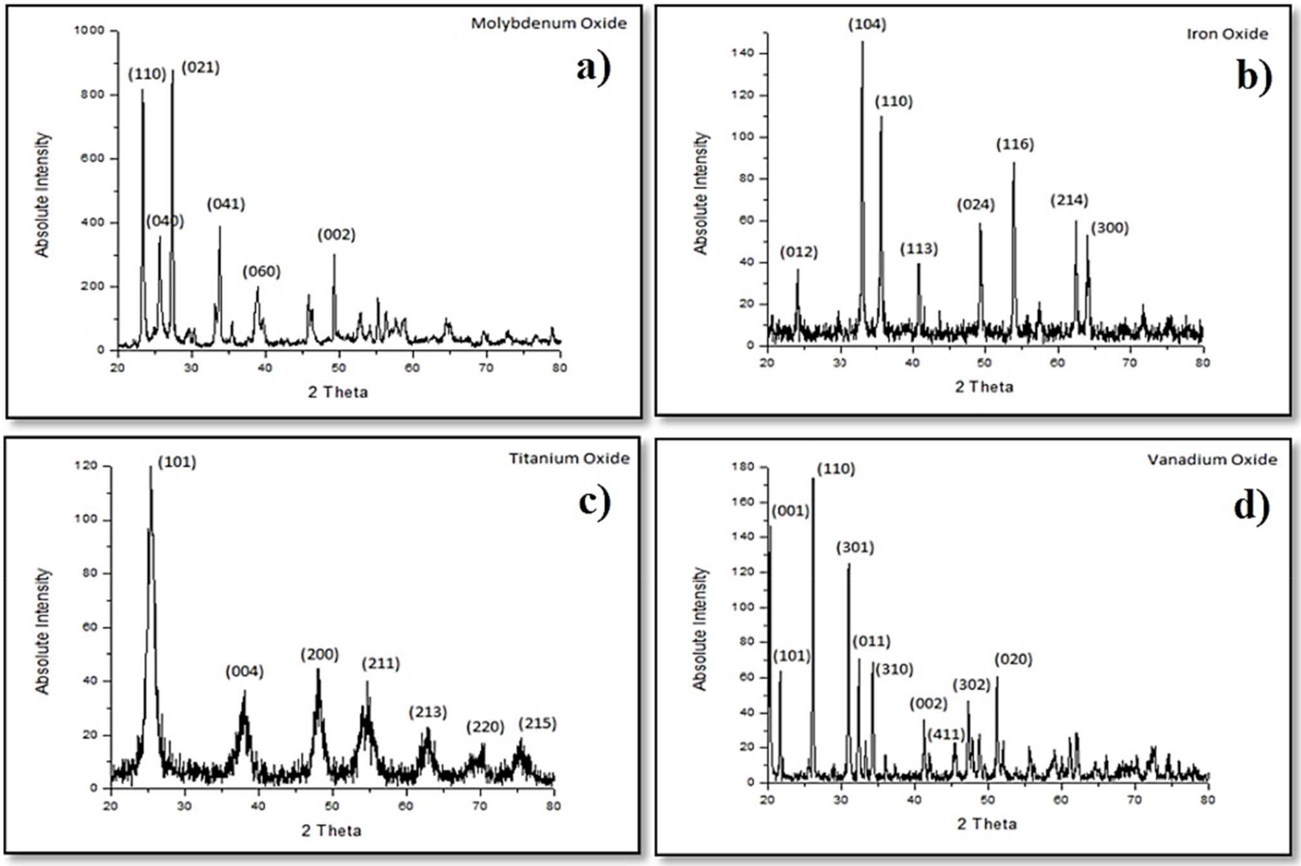

Fig. 5 XRD patterns of (a) molybdenum trioxide (MoO_3) nanoparticles, (b) iron oxide (Fe_2O_3) nanoparticles, (c) titanium oxide (TiO_2) nanoparticles and (d) vanadium pentoxide (V_2O_5) nanoparticles.

electronic configuration of nano-sized particles, which directly depend on the crystallographic phase, particle size and morphology of the catalysts.[28] The present research highlights a limited scope and suggests that further research potential should be explored. Agglomeration can lead to particles composed of smaller crystallites. However, in some synthesis methods, such as hydrothermal synthesis, crystals may grow larger than the agglomerated particle size, especially under specific conditions. An understanding of the effect of crystal size can further be studied by developing a strategy for synthesizing different-sized catalysts.[29] The current work has limitations in this respect. An attempt has been made not solely on particle size but also on critical aspects of crystallite structure that influence reactivity and selectivity in catalytic processes.

Table 2 XRD parameters of the prepared catalysts

Catalyst	Volume of cell (10^6 pm^3)	Density (g cm^{-3})	Crystallite size (nm)
MoO_3	202.99	4.71	43.46
Fe_2O_3	302.72	5.26	58.12
TiO_2	136.92	3.82	63.85
V_2O_5	180.13	3.34	69.21

3.3 Formic acid analysis by high-performance liquid chromatography (HPLC)

HPLC was performed to confirm the formation of formic acid through methanol oxidation using various catalysts involving MoO_3, Fe_2O_3, TiO_2, and V_2O_5. First, standard solutions of different concentrations, *i.e.* 100 ppm, 200 ppm, 300 ppm, 400 ppm, and 500 ppm of formic acid of the highest purity available, were analyzed to obtain the standard peak of formic acid using HPLC (PerkinElmer, Series 200). Different parameters, such as time, flow rate and wavelength, were varied to check their possible effects on the peaks and UV intensities.

HPLC chromatographs showed a better intensity absorbed peak of formic acid using methanol as a solvent system at 210 nm wavelength and 1 ml min^{-1} flow rate at a time ranging from 2.5 to 3.0 minutes. The peak of standard formic acid (purity > 99%) showed a sharp peak, as shown in Fig. 6a. Sample A containing the V_2O_5 nanocatalyst also showed a formic acid peak at the same retention time as the standard formic acid, confirming the formation of formic acid, as shown in Fig. 6b. Sample B containing the MoO_3 nanocatalyst also showed the formic acid peak at the same retention time as the standard formic acid, confirming the formation of formic acid, as shown in Fig. 6c. Sample C containing the Fe_2O_3 nanocatalyst displayed a formic acid peak at the same retention time as the

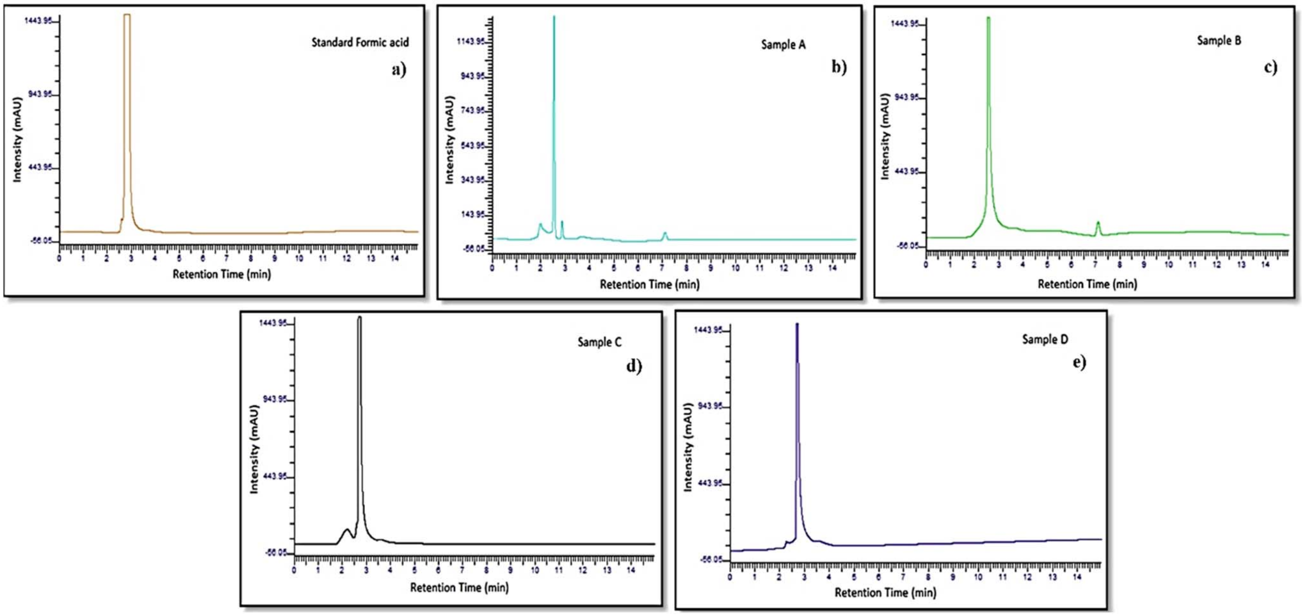

Fig. 6 HPLC chromatographs of (a) standard formic acid (200 ppm), (b) sample A (200 ppm), (c) sample B (200 ppm), (d) sample C (200 ppm) and (e) sample D (200 ppm).

Table 3 HPLC results showing % age yield of formic acid (FA) under employed reaction conditions

Sample	Solvent	Oxidizing agent	Catalyst	Concentration (ppm)	Retention time (min)	Compound	Area (μV s)	Yield (%)
Pure FA	Pure FA	—	—	200	2.55	FA	2.22×10^7	100
Sample A	Methanol	H_2O_2	V_2O_5	200	2.54	FA	5.33×10^6	24
Sample B	Methanol	H_2O_2	MoO_3	200	2.54	FA	2.02×10^7	91
Sample C	Methanol	H_2O_2	Fe_2O_3	200	2.59	FA	1.69×10^7	76
Sample D	Methanol	H_2O_2	TiO_2	200	2.56	FA	1.51×10^7	68

Table 4 Comparison of the prepared catalysts with bench-mark catalysts

Comparison		Catalyst	Reaction process	% age product yield
Prepared catalysts		MoO_3	Oxidation process under UV light	91%
		Fe_2O_3		76%
		TiO_2		68%
		V_2O_5		24%
Bench-mark catalyst	Methanol conversion into formaldehyde	Ag catalyst	BASF process	86.5–90.5%[31]
		Iron-molybdate catalyst	Formox process[30]	88% and 92%[31,32]
	Formaldehyde conversion into formic acid	Titania–vanadia catalyst	Oxidation process	87–88%[14]

standard formic acid, confirming the formation of formic acid, as shown in Fig. 6d. Sample D containing the TiO_2 nanocatalyst showed the formic acid peak at the same retention time as the standard formic acid, confirming the formation of formic acid, as shown in Fig. 6e.

Results given in Table 3 revealed that sample B containing MoO_3 nanocatalyst gave 91% yield of formic acid as suggested by J. Thrane and U. V. Mentzel *et al.*[30] which is the highest among all other nanocatalysts used because molybdenum trioxide is highly specific and catalytically active for maximum conversion of methanol to formic acid *via* oxidation. Table 4 shows a comparison of the results in terms of percentage product yield with those of bench-mark catalysts available for the conversion of methanol into formaldehyde and formic acid.

4 Conclusion

Formic acid has become a viable, low-toxic, and clean H_2 energy source to drive the economy towards a low-carbon future. Fuel cells (FCs) employ formic acid directly to generate power, or indirectly as a source of hydrogen for FCs that produce hydrogen. Formic acid synthesis was successfully carried out in a clean and precisely monitored environment utilizing metal oxide nanocatalysts. Four metal-based oxide nanocatalysts (MoO_3, Fe_2O_3, TiO_2, and V_2O_5) were successfully synthesized using various synthesizing methods, *i.e.* sol–gel, solvothermal, reflux condensation, and ball milling, respectively, and further characterized using different analytical techniques, such as SEM, EDS, and XRD. Batch reactions were performed to evaluate the efficiency of synthesized nanoparticles towards formic acid production from methanol. Owing to their oxidizing qualities toward the generation of formic acid, these metal oxide nanoparticles were employed as catalysts in the oxidation reaction. The product was analyzed using HPLC. The results revealed that metal oxide nanocatalysts exhibited a favourable path toward the formation of formic acid. MoO_3 nanocatalyst gave a 91% yield, which showed the maximum conversion of methanol to formic acid by oxidation reaction. The percentage product yield obtained through this research is almost identical to that obtained through the iron-molybdate catalyst used in the Formox process and the titania–vanadia catalyst used in the oxidation process. Nanocatalysts provided a greater surface area to make the reaction fast and efficient. The overall reaction provided a simple and economical route for methanol oxidation to formic acid. Efficient formic acid production by nanocatalysis offers a plethora of potential uses in the future in various industries, including fuel cell applications, hydrogen storage solutions, and versatile renewable reagents for environmentally friendly and sustainable chemical synthesis.

Data availability

The data that support the findings of this study have been included within this article with proper citation where required.

Author contributions

Mina Arshad: writing-original draft, methodology, and writing-review & editing. Iram Mahmood: supervision. Ali Sarosh: writing-review & editing and validation. Asim Umer: resources and review. Muhammad Athar: writing-review & editing and conceptualization. Mahboob Ahmed Aadil: formal analysis and review.

Conflicts of interest

The authors have declared no conflict of interest.

References

1 *CFR Title 21*, **https://www.accessdata.fda.gov/scripts/cdrh/cfdocs/cfcfr/CFRSearch.cfm?fr=186.1316**.

2 S. B. a. M. Blagoev, *Formic Acid Chemical Economics Handbook*, S&P Global, 2010.

3 M. Milotić, S. Đurić, Z. Čepić, D. Adamović, B. Obrovski, D. Đorđić and M. Stošić, *Processes*, 2022, **10**, 537.

4 Z. Wu, Y. Nie, W. Chen, L. Wu, P. Chen, M. Lu, F. Yu and J. Ji, *Can. J. Chem. Eng.*, 2016, **94**, 1576–1582.

5 A. Han, Z. Zhang, J. Yang, D. Wang and Y. Li, *Small*, 2021, **17**, 2004500.

6 T. H. Mekonnen, T. Ah-Leung, S. Hojabr and R. Berry, *Colloids Surf., A*, 2019, **583**, 123949.

7 R. Schianchi, M. Brena and S. Veraldi, *Int. J. Dermatol.*, 2018, **57**, e3–e4.

8 D. A. Bulushev and J. R. Ross, *ChemSusChem*, 2018, **11**, 821–836.

9 A. Behr and K. Nowakowski, in *Advances in Inorganic Chemistry*, Elsevier, 2014, vol. 66, pp. 223–258.

10 J. Hietala, A. Vuori, P. Johnsson, I. Pollari, W. Reutemann and H. Kieczka, *Ullmann's Encyclopedia of Industrial Chemistry*, 2016, vol. 1, pp. 1–22.

11 F. Schmidt, P. Swiderek, T. Scheele and J. H. Bredehöft, *Phys. Chem. Chem. Phys.*, 2021, **23**, 11649–11662.

12 P. Duarah, D. Haldar, V. Yadav and M. K. Purkait, *J. Environ. Chem. Eng.*, 2021, **9**, 106394.

13 X. Sun, X. Shao, J. Yi, J. Zhang and Y. Liu, *Chemosphere*, 2022, **293**, 133595.

14 T. Andrushkevich, G. Y. Popova, E. Danilevich, I. Zolotarskii, V. Nakrokhin, T. Nikoro, S. Stompel and V. Parmon, *Catal. Ind.*, 2014, **6**, 17–24.

15 N. Thonemann, *Appl. Energy*, 2020, **263**, 114599.

16 Z. Song, D. Han, M. Yang, J. Huang, X. Shao and H. Li, *Appl. Surf. Sci.*, 2023, **607**, 155067.

17 V. Munde, B. D. Bankar, B. B. Mulik, S. S. Zade, A. Biradar and B. R. Sathe, *Appl. Catal., A*, 2024, **681**, 119760.

18 H. Wen, Y. Liu, S. Liu, Z. Peng, X. Wu, H. Yuan, J. Jiang and B. Li, *Small*, 2024, **20**, 2305405.

19 J. A. Kumar, T. Krithiga, S. Manigandan, S. Sathish, A. A. Renita, P. Prakash, B. N. Prasad, T. P. Kumar, M. Rajasimman and A. Hosseini-Bandegharaei, *J. Cleaner Prod.*, 2021, **324**, 129198.

20 S. Mitchell, R. Qin, N. Zheng and J. Pérez-Ramírez, *Nat. Nanotechnol.*, 2021, **16**, 129–139.

21 M. Ikram, M. Rashid, A. Haider, S. Naz, J. Haider, A. Raza, M. Ansar, M. K. Uddin, N. M. Ali and S. S. Ahmed, *Sustainable Mater. Technol.*, 2021, **30**, e00343.

22 S. Mitchell, R. Qin, N. Zheng and J. Pérez-Ramírez, *Nat. Nanotechnol.*, 2021, **16**, 129–139.

23 Y. Zheng, Y. Liu, X. Guo, Z. Chen, W. Zhang, Y. Wang, X. Tang, Y. Zhang and Y. Zhao, *J. Mater. Sci. Technol.*, 2020, **41**, 117–126.

24 N. R. Dighore, P. L. Anandgaonker, S. T. Gaikwad and A. S. Rajbhoj, *Mater. Sci.-Pol.*, 2015, **33**, 163–168.

25 K. Mamatha, C. Ravikumar, H. A. Murthy, V. D. Kumar, A. N. Kumar and A. Jahagirdar, *Sens. Int.*, 2022, **3**, 100153.

26 A. Mansoor, M. T. Khan, M. Mehmood, Z. Khurshid, M. I. Ali and A. Jamal, *Nanomaterials*, 2022, **12**, 1078.

27 S. Rafique, S. M. Abdullah, W. E. Mahmoud, A. A. Al-Ghamdi and K. Sulaiman, *RSC Adv.*, 2016, **6**, 50043–50052.

28 J.-X. Liu, P. Wang, W. Xu and E. J. Hensen, *Engineering*, 2017, **3**, 467–476.

29 J. Xu, Z. Zhang, G. Wang, X. Duan, G. Qian and X. Zhou, *Chem. Eng. Sci.*, 2020, **227**, 115907.

30 J. Thrane, U. V. Mentzel, M. Thorhauge, M. Høj and A. D. Jensen, *Catalysts*, 2021, **11**, 1329.

31 G. Reuss, W. Disteldorf, A. O. Gamer and A. Hilt, *Ullmann's Encyclopedia of Industrial Chemistry*, 2000.

32 H. Gerberich and G. Seaman, *Kirk-Othmer Encyclopedia of Chemical Technology*, John Wiley & Sons, Inc., Hoboken, NJ, USA, 2013, pp. 24–26.